

# Structural and Optoelectronic Characterization of RF Sputtered ZnSnN<sub>2</sub>

Lise Lahourcade, Naomi C. Coronel, Kris T. Delaney, Sujeet K. Shukla, Nicola A. Spaldin, and Harry A. Atwater\*

Terawatt-scale energy demands motivate the investigation of new visible-range direct bandgap semiconductor materials that are abundant and low-cost. Here we demonstrate synthesis of single phase ZnSnN<sub>2</sub> thin films on *c*-plane sapphire and GaN substrates, introducing a new class of zinc- and nitrogen-based semiconductors for visible frequency optoelectronics and photovoltaics. The ZnSnN<sub>2</sub> layers exhibit the wurtzite-derived Pna2<sub>1</sub> orthorhombic structure, in good agreement with *ab initio* calculations. Our electronic structure calculations also indicate a direct bandgap of 1.42 eV at zero Kelvin, which is of high interest for a photovoltaic absorber. Spectroscopic ellipsometry reveals an optical bandgap of about 2 eV and Hall measurements indicate electron concentrations as high as  $\sim 10^{21}$  cm<sup>-3</sup>. These values are consistent with heavy donor doping, where the fundamental bandgap of  $\sim 1.42$  eV at zero Kelvin is altered by a strong Burstein-Moss effect resulting from conduction band filling.

For the past two decades, III-nitride semiconductors (Al<sub>x</sub>Ga<sub>y</sub>In<sub>1-x-y</sub>N) have received considerable attention due to their favorable properties for applications in optoelectronic and electronic devices.<sup>[1,2]</sup> Because of bandgap tunability across the entire visible spectrum and a continuously improving material quantum efficiency, In<sub>x</sub>Ga<sub>1-x</sub>N-based alloys are of increasing interest for new efficient absorber layers in solar cells. In particular, with a bandgap matching the AM1.5 solar spectrum, an In<sub>0.4</sub>Ga<sub>0.6</sub>N absorber layer could reach a maximum theoretical detailed balance efficiency of around 33%. However, the large

lattice mismatch between InN and GaN results in indium segregation and phase separation in high indium content layers, which makes it difficult to fabricate high-quality In<sub>x</sub>Ga<sub>1-x</sub>N with more than 20% indium.<sup>[3,4]</sup> Despite that difficulty, recent progress has been made in low indium content In<sub>x</sub>Ga<sub>1-x</sub>N for solar energy conversion, although the low indium content limits the useful wavelengths to the green and blue spectral regions (<530 nm); today's record external quantum efficiency is 72% with an internal quantum efficiency of 97%, obtained for a solar cell with 12% indium in the active absorber layer.<sup>[5]</sup> However even with future improvements, the cost of indium, being a rather rare metal in the Earth's crust, makes it of potentially limited use for large-scale photovoltaic demands. In this context, we are investigating Zn-IV-N<sub>2</sub> semiconductors, where IV = Sn, Ge, or Si. These materials are expected to exhibit properties that are similar, if not superior, to those of their well-known III-nitride counterparts, with the added benefit of being comprised of earth-abundant materials.<sup>[6,7]</sup> Changing from one group-III element into a combination of group-II and -IV elements is also expected to widen the range of accessible properties. To date, both ZnGeN<sub>2</sub> and ZnSiN<sub>2</sub> have been synthesized and well-characterized. ZnSiN<sub>2</sub> powder was synthesized using high-pressure annealing,<sup>[8]</sup> and thin films have been grown on sapphire, (100) silicon, or silicon carbide by metal-organic chemical vapor deposition (MOCVD).<sup>[9-12]</sup> More extensive efforts were put into ZnGeN<sub>2</sub> fabrication leading to powders made by reaction in a furnace,<sup>[13-15]</sup> single-crystal rods grown using the vapor-liquid-solid method,<sup>[16]</sup> and thin films deposited on glass and silicon by radio frequency (RF) sputter deposition and on sapphire and silicon carbide using MOCVD.<sup>[9,17-19]</sup> On the other hand, thin films of ZnSnN<sub>2</sub> have only recently been grown by RF sputter deposition and molecular beam epitaxy.<sup>[20,21]</sup> Given previous theoretical work and experimental studies on all three materials, we expect direct bandgaps spanning the entire visible spectrum for alloys of ZnSnN<sub>2</sub>, ZnGeN<sub>2</sub> and ZnSiN<sub>2</sub>.<sup>[6,7,9,13-15,17-24]</sup> In light of these predictions, we focus here on the fabrication of ZnSnN<sub>2</sub>, which has not been studied in depth and which is essential to any future Zn-IV-N<sub>2</sub> photovoltaic device.

We initially explored theoretically the most stable structure of bulk ZnSnN<sub>2</sub> by calculating the total energy per unit cell of possible crystal structures derived from those commonly found in nitride binary systems—zinc-blende and wurtzite—with selected Zn/Sn A-site orderings. In III-nitrides, the wurtzite P6<sub>3</sub>mc structure is usually the most stable, and we also expect wurtzite-derived structures to be most stable for ZnSnN<sub>2</sub>. However, while this does turn out to be true, we also find the energetic difference between the different wurtzite- and zinc-blende-derived orderings to be small, suggesting that both phases, or

Dr. L. Lahourcade, N. C. Coronel, Prof. H. A. Atwater  
Thomas J. Watson Laboratories of Applied Physics  
California Institute of Technology  
Pasadena, CA 91125, USA  
E-mail: haa@caltech.edu

Dr. K. T. Delaney  
Materials Research Laboratory  
University of California  
Santa Barbara, CA 93106, USA

S. K. Shukla  
Institute of Quantum Information and Matter  
California Institute of Technology  
Pasadena, CA 91125, USA  
Prof. N. A. Spaldin  
Materials Theory  
ETH Zurich, Wolfgang-Pauli-Strasse 27, 8093 Zurich, Switzerland  
Prof. H. A. Atwater  
Kavli Nanoscience Institute  
California Institute of Technology  
Pasadena, CA 91125, USA



DOI: 10.1002/adma.201204718

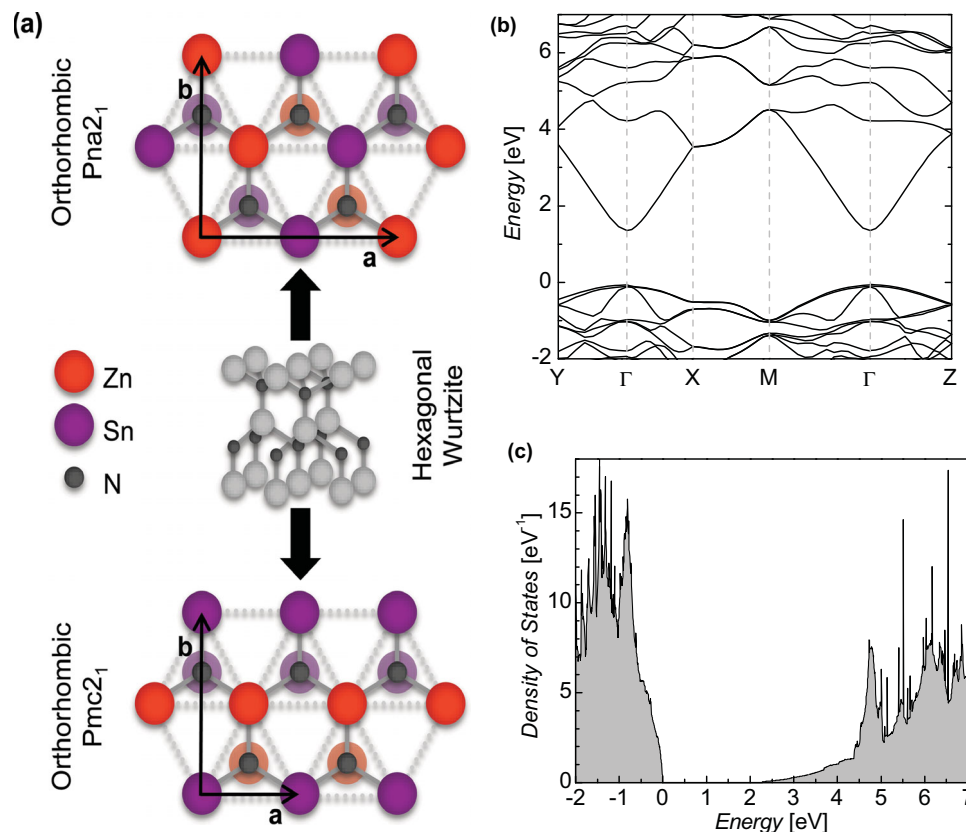


**Figure 1.** Calculated ZnSnN<sub>2</sub> crystallographic & electronic structure. (a) Schematic of the predicted wurtzite-derived structure of ZnSnN<sub>2</sub> including two possible atomic arrangements of the *c*-plane metallic sublayer resulting in the 8-atom Pmc<sub>21</sub> or the 16-atom Pna<sub>21</sub> orthorhombic structures. (b) Band-structure and (c) electronic density of states of orthorhombic Pna<sub>21</sub> ZnSnN<sub>2</sub>, calculated using the HSE06 density functional. The semiconductor is expected to have a direct bandgap of approximately 1.42 eV at zero Kelvin.

indeed random Zn/Sn ordering, could coexist under certain growth conditions. In the wurtzite-derived structure, there are two high-symmetry ways to arrange the Zn and Sn atoms in the hexagonal *c*-plane (Figure 1a), corresponding to the orthorhombic Pmc<sub>21</sub> and Pna<sub>21</sub> space groups. Unfortunately, the two structures, which share many common super groups and differ only in the planar ordering of Zn and Sn atoms, are difficult to experimentally differentiate. We also compared the calculated energy per nitrogen atom for both structures ( $E_{tot}$  in Table 1) and found that any difference in ground-state energy

between the two candidate structures is difficult to resolve. The values of the corresponding lattice parameters at zero Kelvin, calculated using the hybrid HSE06 functional, are also listed in Table 1.<sup>[25,26]</sup>

Our calculated band structure and electronic density of states for orthorhombic ZnSnN<sub>2</sub> in the most stable space group, Pna<sub>21</sub>, are displayed in Figure 1b,c. Our hybrid functional calculations predict a zero Kelvin direct bandgap of 1.42 eV with an uncertainty of about 0.1 eV due to theoretical and numerical approximations. We note that the HSE range of hybrid functionals

**Table 1.** Zero Kelvin equilibrium lattice parameters for the wurtzite-derived Pna<sub>21</sub> and Pmc<sub>21</sub> orthorhombic structures, and electronic properties for the Pna<sub>21</sub> structure, calculated using the hybrid HSE06 functional.

Structure	Lattice Parameters		Electronic Properties				
			Band	$\Delta\epsilon_{VBM}$ [eV]	$m_{xx}^*$	$m_{yy}^*$	$m_{zz}^*$
Pna <sub>21</sub>	$a_0$ [Å]	6.721	CB	1.42	0.14	0.14	0.12
	$b_0$ [Å]	5.842	VB <sub>1</sub>	0.00	0.13	1.98	1.94
	$c_0$ [Å]	5.459	VB <sub>2</sub>	-0.04	2.28	0.14	2.01
	$E_{tot}$ [eV/N]	-10.89	VB <sub>3</sub>	-0.05	2.16	1.71	0.14
	$a_0$ [Å]	3.388					
Pmc <sub>21</sub>	$b_0$ [Å]	5.771					
	$c_0$ [Å]	5.427					
	$E_{tot}$ [eV/N]	-10.89					

contain parameters corresponding to the fraction of non-local exchange and screening length that, when adjusted, affect the predicted bandgap values. Here we fix those parameters to the HSE06 values that have been shown to yield a good quantitative match with experimental data for structural properties and fundamental bandgaps across a wide range of narrow- and intermediate-gap semiconductors, including the group-III nitrides, with a small underestimate for wide-gap semiconductors. Our calculations are therefore free of adjustable parameters. We note that our prediction of the  $\text{ZnSnN}_2$  fundamental bandgap is smaller than recent theoretical work based on the GW method.<sup>[7]</sup> However, we believe that the success of HSE06 for describing the gaps of narrow- and intermediate-gap III-nitrides indicates that we can use this approach as a predictive tool for the fundamental bandgap of this ternary nitride. In wurtzitic III-nitrides, the breaking of cubic crystal symmetry between the  $ab$ -plane and the  $c$ -axis induces a crystal-field splitting of the triply-degenerate valence bands into a doubly-degenerate set and the crystal-field split-off band. Spin-orbit coupling causes further band splittings. In  $\text{ZnSnN}_2$ , which has orthorhombic symmetry produced by the ordering of the mixed 'A' site, the triple degeneracy of the valence bands is entirely lifted due to the crystal-field splitting (Table 1). We do not consider spin-orbit coupling in the present calculations; it is expected to provide only a very weak correction to the fundamental bandgap. Our calculated effective mass for the conduction band is very small and almost isotropic, with a geometric mean of  $0.13 m_0$  (Table 1), which we expect to result in a high electron mobility and therefore good electrical conductivity for  $\text{ZnSnN}_2$ . Although the band-edge hole mobilities are more complicated due to the three distinct sub-bands with widely varying effective masses, in optically excited samples all three valence bands would become populated with carriers, and we note that each of the three bands has a light-hole mass in one crystallographic direction. This feature of the electronic structure may lead to hole mobilities that are also moderately high.

We synthesized thin films of  $\text{ZnSnN}_2$  on  $c$ -plane sapphire and  $c$ -plane GaN template substrates by reactive RF magnetron sputtering from a single  $\text{Zn}_{0.75}\text{Sn}_{0.25}$  target or from Zn and Sn elemental targets at around  $250^\circ\text{C}$  in an atmosphere of argon and nitrogen gases. Energy dispersive X-ray spectroscopy confirms the deposition of stoichiometric material within the error

of the instrument. To determine the phase of our material, we measured powder diffraction patterns from a ground up thick film that was removed from the substrate (Figure 2a). The theoretical peak positions based on our calculated zero Kelvin lattice parameters for  $\text{Pna}2_1$ ,  $\text{Pmc}2_1$ , and an average wurtzite structure, representing a random distribution of Zn and Sn atoms, are also shown in Figure 2a for comparison. The pattern from our material matches well with the  $\text{Pna}2_1$  and average wurtzite structures, where the most apparent distinguishing feature is a slight splitting of some peaks when moving from the average structure to the  $\text{Pna}2_1$  structure. Although it appears that our material only exhibits single peaks, it should be noted that the full width at half maximum (FWHM) of the peaks that would be split in the  $\text{Pna}2_1$  case is large compared to the peaks that do not split (Figure 2a). For this reason, we have concluded that the  $\text{Pna}2_1$  space group describes the predominant arrangement of metallic atoms in our material. This is consistent with reports on synthesis of  $\text{ZnGeN}_2$  and  $\text{ZnSiN}_2$  materials where several groups have shown that they both exhibit the  $\text{Pna}2_1$  structure.<sup>[8,15,18,24,27]</sup>

Figure 2b compares the X-ray diffraction (XRD) measurements of  $\text{ZnSnN}_2$  layers deposited under the same conditions on  $c$ -plane sapphire and GaN, wherein we attribute the peak at  $2\theta \sim 32.5^\circ$  to  $\text{ZnSnN}_2(002)$ . The layers deposited on top of GaN templates not only exhibit a much sharper (002) peak, with a FWHM reduced by a factor of two compared to layers deposited on sapphire, but also show a slight shift in the peak position towards larger  $2\theta$  angles. Both can be seen as consequences of the large difference in the lattice mismatch between the layer on GaN ( $\sim 6.5\%$ ) and the layer on sapphire ( $\sim 29\%$ ). Based on these XRD measurements for various stoichiometric samples, we have measured a  $c$  lattice parameter of  $5.52 \pm 0.01 \text{ \AA}$ . We cannot determine the  $a$  or  $b$  parameters from these measurements because the films are textured in the (001) direction. Hall measurements performed on the layers reveal  $n$ -type material, with electron concentrations ranging from  $\sim 5 \times 10^{19} \text{ cm}^{-3}$  to  $\sim 1 \times 10^{21} \text{ cm}^{-3}$ . From our band structure calculations, we expect to have a high electron mobility material, but we instead find mobilities of about  $10 \text{ cm}^2 \text{ V}^{-1} \text{ s}^{-1}$  or lower. We believe this low mobility is due in part to the small grain size, which is typical for materials grown by sputtering. Another factor influencing the observed electron mobility could be a subtle band-filling

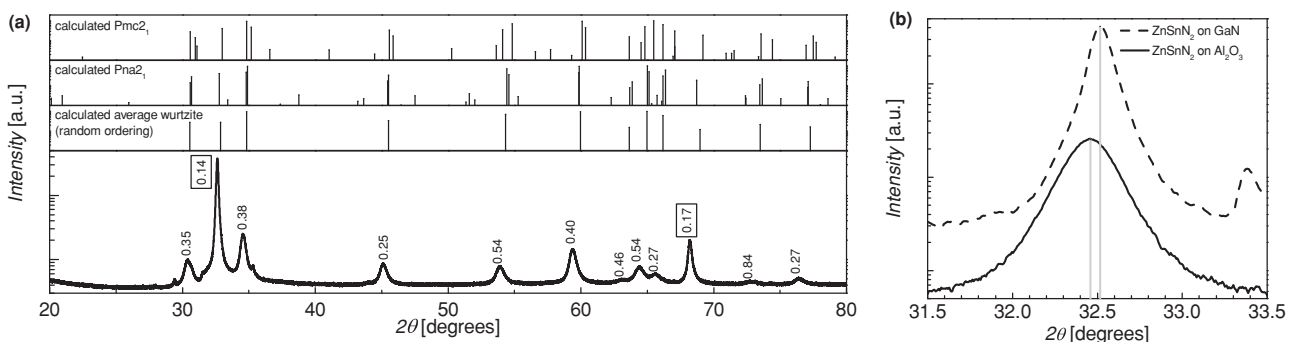


**Figure 2.** Determination of  $\text{ZnSnN}_2$  structure. (a) Powder diffraction spectrum of  $\text{ZnSnN}_2$  and peak positions calculated from zero Kelvin lattice parameters for the  $\text{Pmc}2_1$ ,  $\text{Pna}2_1$ , and average wurtzite structures. The labels on the peaks are an indication of the FWHM, and the boxes highlight the peaks that do not split in the lower symmetry orthorhombic structures. (b) X-ray diffractograms of (001)-oriented layers deposited under the optimized conditions on both  $c$ -plane sapphire and GaN.

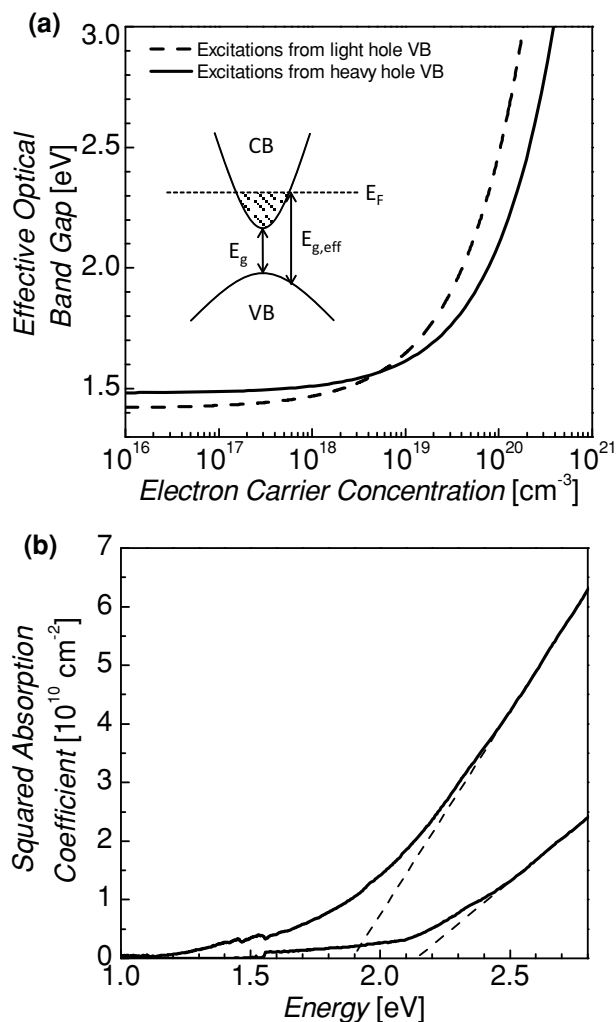


**Figure 3.** Burstein-Moss effect in ZnSnN<sub>2</sub>. (a) Calculated shift of the optical bandgap with the electron doping concentration; as shown in the inset, strong *n*-type doping of ZnSnN<sub>2</sub> leads to conduction band filling and the resulting Burstein-Moss effect, wherein the effective bandgap lies at a higher energy than the fundamental bandgap. (b) Absorption edge extrapolation from spectroscopic ellipsometry measurements of two different samples; the sample with the smaller extrapolated energy was deposited with a higher power resulting in non-oriented polycrystalline growth. The linear dependence of  $\alpha^2$  versus the photon energy is typical of a direct bandgap semiconductor.

effect, originating from the anharmonic nature of the conduction band at moderate non-zero crystal momenta. The band anharmonicity leads to a momentum-dependent effective mass, such that the cyclotron (transport) and band-edge effective masses differ appreciably (Figure 1b).

For further study of the electronic structure, we used spectroscopic ellipsometry measurements to reveal features in the joint density of states, particularly the optical bandgap. For direct bandgap semiconductors, the square of the absorption coefficient ( $\alpha^2$ ) versus photon energy can be linearly extrapolated to the energy axis to estimate the value of the bandgap. In Figure 3b, we present two samples deposited by co-sputtering. Both samples shown are stoichiometric and intrinsically *n*-doped

with electron concentrations in the range previously stated. The linear fit of our data near the absorption edge reveals a measured direct optical bandgap for ZnSnN<sub>2</sub> of ~1.9 eV and ~2.2 eV for the two samples presented. At first glance, our measured values of the bandgap seem to be consistent with the recently reported theoretical bandgap of 2.02 eV.<sup>[7]</sup> However, the high carrier concentration in our sample combined with the low conduction band effective mass *must* incur a large Burstein-Moss effect in the apparent optical gap. As illustrated in Figure 3a, free electrons will fill the bottom of the conduction band, pinning the Fermi level to energies above the conduction band edge, and consequently blocking low-energy optical excitations to yield a measured gap that is larger in energy than the underlying fundamental bandgap of the material. As an example, the bandgap initially reported for InN (1.9–2.1 eV), which is larger than the now-accepted gap of approximately 0.69 eV, has largely been attributed to this effect.<sup>[28,29]</sup> The calculated effective optical bandgap depending on electron concentration (Figure 3a), based on our calculated band structure (Figure 1b), indicates that we should expect a gap of at least 1.8 eV for the electron concentrations we measured. Ultimately, we cannot assign a precise experimental value of the fundamental bandgap until we are able to significantly reduce the unintentional doping concentration in our material, but our combined theoretical and experimental study points to a fundamental gap in the red-green spectral region.

In conclusion, we have synthesized thin films of stoichiometric ZnSnN<sub>2</sub> that exhibit the predicted Pna2<sub>1</sub> wurtzite-derived orthorhombic crystal structure. Our material has a measured optical absorption edge near 2 eV, which is higher in energy than our theoretically predicted value of 1.42 eV. This difference is attributed to the Burstein-Moss effect, which is evidenced by large electron carrier concentrations according to Hall measurements. We believe that the findings of this study demonstrate the feasibility of fabricating stoichiometric, single-phase ZnSnN<sub>2</sub>, a new earth-abundant small bandgap semiconductor. These first optoelectronic measurements are promising for future applications, especially in photovoltaics and solid-state lighting.

## Experimental Section

**Reactive RF Magnetron Sputter Deposition:** Thin films were synthesized in an AJA International sputtering chamber, with a background pressure in the high 10<sup>-8</sup> Torr. The reactive RF plasma was created from a mixture of argon and nitrogen gases kept at 3 mTorr. The materials were deposited on *c*-sapphire and LUMILOG *c*-GaN template substrates at around 250 °C from a Zn<sub>0.75</sub>Sn<sub>0.25</sub> target or from Zn and Sn elemental targets. Applied powers ranged from 44 W to 164 W.

**X-Ray Diffraction (XRD):** The structure and phase of our material was studied by XRD with a PANalytical X'Pert diffractometer using a Cu K $\alpha$  source ( $\lambda = 1.5406$  Å) over a  $2\theta$  range of 20° to 80° for the powder spectrum and 30° to 43° for the thin films on a substrate.

**Energy Dispersive X-ray Spectroscopy (EDS):** Composition measurements were performed using a ZEISS 1550 VP field emission scanning electron microscope equipped with an Oxford INCA Energy 300 EDS System and an accelerating voltage of up to 7 kV.

**Spectroscopic Ellipsometry:** Spectroscopic ellipsometry was performed on samples grown on *c*-sapphire at incidence angles of 50°, 60°, and 70° for 250 nm <  $\lambda$  < 2300 nm with a Xe lamp visible light source and a Fourier-transform infrared spectrometer. The wavelength-dependent complex refractive index was fit from the measured Fourier coefficients at 1 nm intervals using a fixedNK model.

**Computational methods:** We computed structural and electronic properties using plane-wave density functional theory as implemented in the Vienna *ab initio* Simulation Package (VASP).<sup>[30]</sup> Our chosen exchange-correlation functional is the hybrid HSE06,<sup>[31]</sup> which has been demonstrated to reproduce both ground-state properties and fundamental gaps with high accuracy.<sup>[32]</sup> The core-valence partitioning is handled using the projector-augmented wave method, with datasets parameterized using the PBE-GGA functional. Our wave functions were computed with periodic boundary conditions and expanded using a plane-wave basis with an energy cutoff of 800 eV. Our tolerance for iterative improvement of the wave functions was  $10^{-8}$  eV in both the total energy and electronic eigenvalues. The first Brillouin zone was discretely sampled using a  $4 \times 4 \times 4$  Monkhorst-Pack mesh.<sup>[33]</sup> The atomic structure was relaxed using a quasi-Newton algorithm until all force components were less than  $10^{-4}$  eV  $\text{\AA}^{-1}$ . Further technical details will be reported elsewhere.<sup>[34]</sup>

## Supporting Information

Supporting Information is available from the Wiley Online Library or from the author.

## Acknowledgements

This work was supported in part by the US Department of Energy under grant DE-FG02-07ER46405, and in part by the DOW Chemical Company.

Received: November 15, 2012

Revised: December 6, 2012

Published online:

- [1] S. Nakamura, S. J. Pearton, G. Fasol, *The Blue Laser Diode: The Complete Story*, 2nd ed., Springer, Berlin **2000**.
- [2] S. J. Pearton, C. R. Abernathy, F. Ren, *Gallium Nitride Processing for Electronics, Sensors, and Spintronics*, Springer, New York **2006**.
- [3] N. Duxbury, U. Bangert, P. Dawson, E. J. Thrush, W. Van der Stricht, K. Jacobs, I. Moerman, *Appl. Phys. Lett.* **2000**, *76*, 1600.
- [4] Z. Liliental-Weber, D. N. Zakharov, K. M. Yu, J. W. Ager, W. Walukiewicz, E. E. Haller, H. Lu, W. J. Schaff, *J. Electron Microsc.* **2005**, *54*, 243.
- [5] E. Matioli, C. Neufeld, M. Iza, S. C. Cruz, A. A. Al-Heji, X. Chen, R. M. Farrell, S. Keller, S. DenBaars, U. Mishra, S. Nakamura, J. Speck, C. Weisbuch, *Appl. Phys. Lett.* **2011**, *98*, 021102.
- [6] T. R. Paudel, W. R. L. Lambrecht, *Phys. Rev. B* **2009**, *79*, 245205.
- [7] A. Punya, W. R. L. Lambrecht, M. van Schilfgaarde, *Phys. Rev. B* **2011**, *84*, 165204.
- [8] T. Endo, Y. Sato, H. Takizawa, M. Shimada, *J. Mater. Sci. Lett.* **1992**, *11*, 424.
- [9] A. Osinsky, V. Fuflyigin, L. D. Zhu, A. B. Goulakov, J. W. Graff, E. F. Schubert, in *Proc. of the IEEE/Cornell Conference on High Performance Devices* **2000**, 168.
- [10] T. Cloitre, A. Sere, R. L. Aulombard, *Superlattice Microst.* **2004**, *36*, 377.
- [11] A. Mintairov, J. Merz, A. Osinsky, V. Fuflyigin, L. D. Zhu, *Appl. Phys. Lett.* **2000**, *76*, 2517.
- [12] S. J. Pearton, M. E. Overberg, C. R. Abernathy, N. A. Theodoropoulou, A. F. Hebard, S. N. G. Chu, A. Osinsky, V. Fuflyigin, L. D. Zhu, A. Y. Polyakov, R. G. Wilson, *J. Appl. Phys.* **2002**, *92*, 2047.
- [13] K. Du, C. Bekele, C. C. Hayman, J. C. Angus, P. Piruz, K. Kash, *J. Cryst. Growth*. **2008**, *310*, 1057.
- [14] W. L. Larson, H. P. Maruska, D. A. Stevenson, *J. Electrochem. Soc.* **1974**, *121*, 1673.
- [15] R. Viennois, T. Taliercio, V. Potin, A. Errebah, B. Gil, S. Charar, A. Haidoux, J. C. Tedenac, *Mat. Sci. Eng. B-Solid* **2001**, *82*, 45.
- [16] T. J. Peshek, T. R. Paudel, K. Kash, W. R. L. Lambrecht, *Phys. Rev. B* **2008**, *77*, 235213.
- [17] S. Kikkawa, H. Morisaka, *Solid State Commun.* **1999**, *112*, 513.
- [18] T. Misaki, A. Wakahara, H. Okada, A. Yoshida, *J. Cryst. Growth*. **2004**, *260*, 125.
- [19] L. D. Zhu, P. H. Maruska, P. E. Norris, P. W. Yip, L. O. Bouthillette, *MRS Internet J. Nitride Semicond. Res.* **1999**, *4*, G3.8.
- [20] N. C. Coronel, L. Lahourcade, K. T. Delaney, A. M. Shing, H. A. Atwater, in *Proc. of the 38<sup>th</sup> IEEE Photovoltaic Specialists Conference* **2012**, 3204.
- [21] N. Feldberg, B. Keen, J. D. Aldous, D. O. Scanlon, P. A. Stampe, R. J. Kennedy, R. J. Reeves, T. D. Veal, S. M. Durbin, in *Proc. of the 38<sup>th</sup> IEEE Photovoltaic Specialists Conference* **2012**, 2524.
- [22] S. Limpijumngong, S. N. Rashkeev, W. R. L. Lambrecht, *MRS Internet J. Nitride Semicond. Res.* **1999**, *4S1*, G6.11.
- [23] V. L. Shaposhnikov, A. V. Krivosheeva, F. A. D'Avitaya, J. L. Lazzari, V. E. Borisenko, *Phys. Status Solidi B* **2008**, *245*, 142.
- [24] Q. H. Zhang, J. Wang, C. W. Yeh, W. C. Ke, R. S. Liu, J. K. Tang, M. B. Xie, H. B. Liang, Q. Su, *Acta Mater.* **2010**, *58*, 6728.
- [25] A. V. Krukau, O. A. Vydrov, A. F. Izmaylov, G. E. Scuseria, *J. Chem. Phys.* **2006**, *125*, 224106.
- [26] J. P. Perdew, K. Burke, M. Ernzerhof, *Phys. Rev. Lett.* **1996**, *77*, 3865.
- [27] M. Wintenberger, M. Maunay, Y. Laurent, *Mater. Res. Bull.* **1973**, *8*, 1049.
- [28] V. Y. Davydov, A. A. Klochikhin, R. P. Seisyan, V. V. Emtsev, S. V. Ivanov, F. Bechstedt, J. Furthmüller, H. Harima, A. V. Mudryi, J. Aderhold, O. Semchinova, J. Graul, *Phys. Status Solidi B* **2002**, *229*, R1.
- [29] J. Wu, W. Walukiewicz, K. M. Yu, J. W. Ager, E. E. Haller, H. Lu, W. J. Schaff, Y. Saito, Y. Nanishi, *Appl. Phys. Lett.* **2002**, *80*, 3967.
- [30] G. Kresse, J. Furthmüller, *Phys. Rev. B* **1996**, *54*, 11169.
- [31] J. Heyd, G. E. Scuseria, M. Ernzerhof, *J. Chem. Phys.* **2006**, *124*, 219906.
- [32] Q. M. Yan, P. Rinke, M. Scheffler, C. G. Van de Walle, *Appl. Phys. Lett.* **2009**, *95*, 121111.
- [33] H. J. Monkhorst, J. D. Pack, *Phys. Rev. B* **1976**, *13*, 5188.
- [34] K. T. Delaney, S. K. Shukla, N. A. Spaldin, to be submitted.